JOURNAL OF CATALYSIS 120, 387–400 (1989)

Preparation, Characterization, and Activity of Fluorinated Aluminas for Halogen Exchange

R. I. HEGDE AND M. A. BARTEAU[1]

Center for Catalytic Science and Technology, Department of Chemical Engineering, University of Delaware, Newark, Delaware 19716

Received June 6, 1989

Fluorinated aluminas with α-AlF_3 contents up to 90+% were prepared by treatment with the fluoroalkanes CHF_3 or C_2HF_5 at 773 K. XPS results suggest that nearly complete fluorination of the surface occurs even at low extents of bulk fluorination. Neither γ-Al_2O_3 nor α-AlF_3 exhibits significant activity for reaction of CHF_3 following adsorption at 300 K and subsequent temperature-programmed desorption. In contrast, partially fluorinated aluminas strongly adsorb CHF_3, $CHClF_2$, and $CHCl_2F$. TPD experiments indicate that all three C_1-HCFCs desorb from partially fluorinated alumina above 500 K; all react to liberate HF and CO_2, and the chlorine-containing species undergo fluorine-for-chlorine exchange to produce CHF_3. These results suggest that halogen-exchange reactions of HCFCs can be carried out with materials resembling conventional fluorination catalysts.

INTRODUCTION

Chlorofluorocarbons (CFCs) find widespread use in modern society as refrigerants, solvents, and blowing agents. Owing in part to the discovery of a "hole" in the Earth's ozone layer over Antarctica and to the observation of decreasing levels of stratospheric ozone (*1*), there has been a rising tide of international concern over the release of these substances into the atmosphere. The Montreal Protocol mandates 50% cuts in the production of CFCs by 1998. Recently published models of atmospheric chemistry have suggested that even greater production cuts are needed to decrease the level of ozone-depleting atmospheric chlorine (*2*), prompting calls for the elimination of production of these molecules. There is a compelling need, not only to identify "safe" replacements for the CFCs currently in widespread use, but also to develop viable routes for their production.

Perhaps not surprisingly, the properties which render some fluorocarbons environmentally attractive alternatives also render them more difficult to manufacture. One approach to the environmental problem is to reduce the chlorine content of existing CFCs, primarily by replacement of chlorine atoms with hydrogen atoms in these molecules. Proposed substitutions include CF_3CFH_2 (HCFC-134a) and $CHClF_2$ (HCFC-22) for CCl_2F_2 (CFC-12) in refrigeration applications, and CF_3CHCl_2 (HCFC-123) and CCl_2FCH_3 (HCFC-141b) for CCl_3F (CFC-11) in foam-blowing applications (*3*). Hydrogen-containing chlorofluorocarbons and fluorocarbons are much more chemically reactive than their fully halogenated analogs, and the usual hypothesis is that they will degrade before reaching the upper atmosphere to react with ozone. However, this same reactivity renders these molecules more vulnerable to undesirable side reactions in typical catalytic fluorination processes. These side reactions include "over-fluorination" to fully halogenated derivatives and dehydrogenation to unsaturated species which may adsorb

[1] To whom correspondence should be addressed.

0021-9517/89 $3.00

strongly on the catalyst and result in its deactivation.

The technology of catalytic fluorination for CFC production has existed since the 1930s and there is considerable incentive to modify it for production of their replacements by altering the catalyst to achieve higher selectivity toward the desired HCFCs. Limited information available in the patient literature (*4*) suggests that such a strategy is feasible. Unfortunately the relevant chemistry has been largely neglected, and there currently exists little guidance for such catalyst redesign.

Chlorofluorocarbons are typically produced by reaction of chlorocarbons with HF, catalyzed by fluorinated oxides, typically Al_2O_3 or Cr_2O_3 promoted with other metal cations (*5, 6*). For fully halogenated ethanes, no fewer than 10 different products are possible; these have chemical formulas C_2Cl_6, C_2Cl_5F, $C_2Cl_4F_2$ (two isomers), $C_2Cl_3F_3$ (two isomers), $C_2Cl_2F_4$ (two isomers), C_2ClF_5, and C_2F_6. The product distribution is influenced by the intrinsic properties of these molecules, by their interaction with the catalyst and the surface reactions occurring on the catalyst, and finally by the process conditions. There is little agreement as to the network of reactions which connects these molecules, and virtually nothing is known about their interaction with the surface and the mechanisms of catalyst function. If one now introduces hydrogen, the potential product distribution increases in complexity, and one adds the chemical hurdles of carrying out fluorine-for-chlorine exchange without removal of the hydrogen, or of hydrogen-for-chlorine exchange without altering the fluorine distribution. The catalytic strategies one might employ are those borrowed from the analogous selective oxidation of hydrocarbons. One can attempt to control the selectivity by control of the availability of fluorine on the catalyst, or one can modify the catalyst to discriminate against adsorption (and therefore reaction) of the desired products once formed. Optimal catalysts are likely to employ both strategies to some extent.

Fluorination of alumina increases the catalytic activity for other classes of reactions, especially acid-catalyzed conversions of hydrocarbons such as cracking, isomerization, polymerization, and disproportionation (*7–10*). In these applications, fluorination of alumina with hydrofluoric acid, ammonium fluoride, or ammonium bifluoride is the common practice. The catalytic properties of these fluorinated aluminas have been documented (*11–16*). However, the fluorination of alumina by different methods and the structure–property relationships of the resulting materials have not been widely explored. A comparison of physical and chemical properties of fluorinated aluminas prepared by treatment with trifluoromethane vs hydrofluoric acid was recently reported (*17*). Fluorination of alumina with fluoroalkanes offers distinct advantages over the standard HF fluorination method with respect to ease of handling, provided that the resulting material is catalytically active.

This work reports the following: (1) the preparation and characterization of fluorinated aluminas with different fluorine contents and crystallite sizes by reacting alumina with fluoroalkanes (CHF_3 and C_2HF_5) and (2) the adsorption behavior and surface reactions of C_1-CFCs: CHF_3 (HCFC-23), $CHClF_2$ (HCFC-22), $CHCl_2F$ (HCFC-21) and CCl_2F_2 (CFC-12), on these fluorinated aluminas. The goal of this research is an understanding of the catalyst requirements and reaction pathways for formation of representative HCFCs.

EXPERIMENTAL

The alumina powder used in this investigation consisted of a commercial γ-alumina supplied by Du Pont, which was ground to a fine powder (20–40 mesh). The chlorofluorocarbon gases used in these experiments (all 99.0% purity) were trifluoromethane (HCFC-23), chlorodifluoromethane (HCFC-22), dichlorofluoromethane

(HCFC-21), and dichlorodifluoromethane (CFC-12). These were used as supplied by SCM Specialty Chemicals. He (99.995%), used as the carrier gas for the flow reactor system, was further purified by passing through a 5-Å molecular sieve trap at room temperature, a Harshaw deoxygenation trap (supported CuO) at room temperature, and finally a molecular sieve trap at 77 K.

Fluorinated aluminas with different extents of fluorination were prepared by reacting the alumina powder with the gaseous fluoroalkanes CHF_3 and C_2HF_5. These fluoroalkanes contain relatively weak C–H bonds (106 kcal/mol) and strong C–F bonds (130 kcal/mol) (*18*). It has been suggested that the initial reaction involves cleavage of the C–H bond leading to water formation, with subsequent complete degradation of the fluoroalkyl moieties. This decomposition reaction produces aluminum fluoride (*17*). The borosilicate quartz U-tube reactor used for both sample fluorination and TPD experiments was described in detail previously (*19*). The sample bed was supported on a 60-μm sintered glass frit and the reactor was operated in a down-flow mode. The temperature in the reactor was measured with a type-K thermocouple [Omega (SCASS-0620), outside diameter 1.5 mm]. The thermocouple entered the reactor through a stainless-steel Cajon fitting and penetrated to the middle of the sample bed. The response of the thermocouple to a step change in the temperature was measured and the time constant was found to be about 5 s. The thermocouple signal was linearized and converted to a 1-mV/K analog output signal by an Omega Model 199 thermocouple readout. A Chemical Data Systems temperature programmer (Model 210) and Hoskins FA-120 crucible furnace were used to heat the reactor at linear rates ranging from 1 to 30 K/min. A small portion (typically, 30 ml/min) of the reactor exit gas was directed through a molecular jet separator to a differentially pumped UTI-100C quadrupole mass spectrometer for analysis.

Temperature-programmed desorption spectra of various HCFCs from powder samples were obtained with the same apparatus. In these experiments, approximately 50–100 mg of the sample was placed on the glass frit within the quartz U-tube reactor. The powder sample was activated by heating to 773 K and cooling to room temperature in flowing He (30 ml/min) before adsorption. The sample was then exposed to the HCFC gas at room temperature through a four-port valve. After the desired exposure was reached, the sample was purged with He (30 ml/min) in order to remove the residual gases from the walls of the reactor assembly, as well as any unreacted HCFC from the sample surface. After sufficient purging the reactor was enclosed within the tubular furnace and heated at a programmed rate of 12.5 K/min to a maximum temperature of 773 K in TPD experiments. A portion of the reactor exit gas was directed to the mass spectrometer for analysis. The spectrometer was capable of measuring ion mass to charge ratios (m/e) between 1 to 300 with unity resolution. A differentially pumped jet separator inlet system (Scientific Glass Engineering, Inc.), operating at 0.2 mTorr, was used to introduce a sample of the reactor effluent directly into the ionization region of the mass spectrometer. With a 30-ml/min flow of He through the inlet system, the operating pressure inside the mass spectrometer was about 2×10^{-6} Torr. An IBM-PC interfaced through a TecMar PC-LabMaster system was used to control the spectrometer and acquire TPD data, including the reactor thermocouple signal from the Omega 199 readout.

X-ray diffraction patterns of the powder samples were recorded at room temperature on a Philips automated X-ray diffractometer using nickel-filtered Cu$K\alpha$ radiation (1.5404 Å). The X-ray tube was operated at 45 kV and 40 mA. Samples were finely ground and packed into a plastic holder with an $18 \times 18 \times 2$-mm opening. XRD was used to determine bulk crystalline phases and crystallite sizes of various alumina

samples. Determination of crystallite sizes of the alumina samples was based on XRD line broadening. Mean crystallite sizes were calculated from the Scherrer equation (*20*) based on the width of the α-AlF_3 (220) and γ-Al_2O_3 (220) and γ-Al_2O_3 (440) lines.

The BET surface areas of the samples were determined by means of low temperature adsorption of nitrogen using an OMNISORP 100 (Omicron Technology). The samples were outgassed under vacuum ($P < 10^{-5}$ Torr) at 623 K for 5 hr before the measurement.

X-ray photoelectron spectroscopy was employed to determine the surface composition of the fluorinated alumina samples. XPS spectra were obtained using a Physical Electronics Model 550 Electron Spectrometer equipped with an aluminum anode (Al$K\alpha$ = 1486.6 eV) operated at 10 kV and 60 mA. No special treatments were applied to the samples in the UHV chamber. After scanning the overall spectrum, the individual peaks were recorded in detail by accumulation of data from multiple scans. All binding energies were referenced to the C(1*s*) peak at 284.6 eV. The residual pressure inside the analysis chamber was less than 1×10^{-9} Torr.

RESULTS

Preparation and Characterization of Aluminas Fluorinated with Fluoroalkanes

A series of fluorinated aluminas [designated Al_2O_3, Al_2O_3(F), and AlF_3] was prepared by activating approximately 100–200 mg of the alumina powder at 773 K in the quartz U-tube reactor in flowing He (30 ml/min), followed by treatment with a stream (15–30 ml/min) of gaseous fluoroalkane (CHF_3 or C_2HF_5) at 773 K for a specified time. This fluorination method is similar to that described by McVicker *et al.* (*17*). The sample, designated as Al_2O_3(DF), was prepared by the conventional method, i.e., treatment of alumina with HF, and used as supplied by Du Pont.

TABLE 1

Fluorination of γ-Al_2O_3 with CHF_3[a]

Sample	Fluorination temperature (K)	Fluorination time (hr)	Bulk fluoride content[b] (% AlF_3)	Surface area (m^2/g)
Al_2O_3	—	—	0	202
Al_2O_3(F)	773	3.0	40+	52
AlF_3	773	8.0	90+	18
Al_2O_3(DF)[c]			90+	28

[a] CHF_3 (15–30 ml/min) with a total pressure of 1 atm was used in each fluorination.
[b] Fluoride content estimated by XRD.
[c] Sample treated with HF, see text.

This fluoroalkane fluorination method could be utilized to produce partially fluorinated alumina, designated Al_2O_3(F), as well as fully fluorinated alumina, designated AlF_3, depending on the fluoroalkane treatment time (see Table 1). An important feature of this fluorination method is the possibility of preparing mixtures of aluminum oxide and aluminum fluoride of varying bulk composition simply by regulating the fluoroalkane consumption in such a way that the desired end product is obtained. The fluorination of Al_2O_3 was monitored by the evolution of H_2O and CO by mass spectrometry. XRD and XPS measurements confirmed the fluorination of the solid.

The X-ray diffraction (XRD) patterns of the as-supplied Al_2O_3 and Al_2O_3(DF) samples, as well as the samples fluorinated by fluoroalkane treatment, were recorded (see Fig. 1), and the results are summarized in Table 2. Pure alumina gave diffraction lines characteristic of the γ-Al_2O_3 phase.

TABLE 2

XRD Characterization of Fluorinated Aluminas

Sample	Bulk phase	Crystallite size (Å)
Al_2O_3	γ-Al_2O_3	55
Al_2O_3(F)	α-AlF_3 and γ-Al_2O_3	115
AlF_3	α-AlF_3	155
Al_2O_3(DF)	α-AlF_3	155

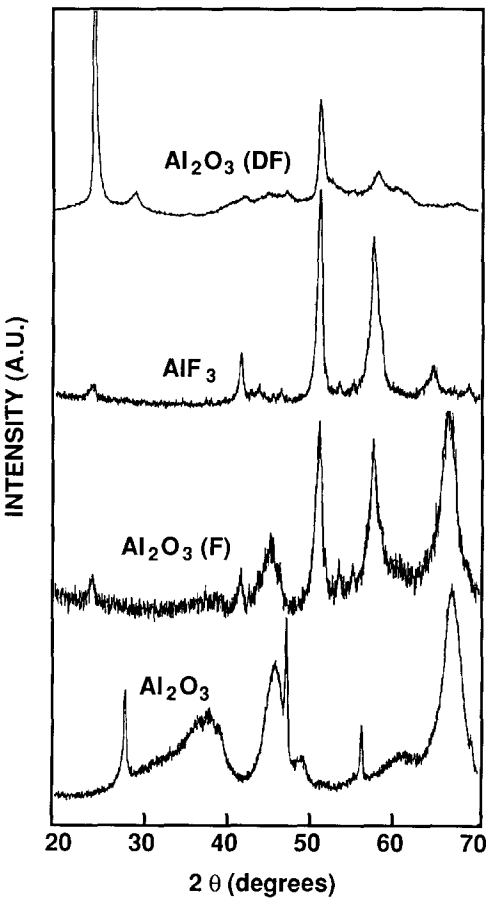

FIG. 1. X-ray diffraction patterns for γ-Al_2O_3, partially fluorinated alumina $Al_2O_3(F)$, and fully fluorinated aluminas, AlF_3 and $Al_2O_3(DF)$.

The three sharpest lines in this pattern were due to silicon added as a calibration standard. The average crystallite size of the γ-alumina was calculated to be 55 Å from the width of the $2\theta = 66.76°$ X-ray line.

The XRD pattern of the partially fluorinated alumina $Al_2O_3(F)$ indicated the presence of both α-AlF_3 and γ-Al_2O_3. Formation of both AlF_3 and Al_2O_3 during fluorination of alumina with fluoroalkanes is consistent with the observations of McVicker *et al.* (*17*). Similar results have been obtained by others (*12, 16, 21, 22*) by reacting alumina with fluorine sources other than fluoroalkanes around 825 K. There were no XRD lines characteristic of β-AlF_3, γ-AlF_3, or other fluoride phases in our samples. From a comparison of XRD line intensities of pure γ-Al_2O_3 and $Al_2O_3(F)$ recorded under identical conditions, the α-AlF_3 content in the $Al_2O_3(F)$ was estimated to be ca. 40–50%. The average crystallite size of the $Al_2O_3(F)$ sample was calculated to be 115 Å using the width of the (220) line with $2\theta = 51.08°$.

For AlF_3, the XRD pattern indicated the presence of only the α-AlF_3 phase. No other aluminum fluoride, oxide, or oxyfluoride phases could be detected. Thus the X-ray diffraction pattern verified the complete transformation of γ-Al_2O_3 into α-AlF_3. The width of the 2θ X-ray line from AlF_3 was somewhat narrower than that from $Al_2O_3(F)$. The average crystallite sizes (see Table 2) of α-AlF_3 were calculated to be 155 Å using the width of the (220) X-ray line. These XRD results are in good agreement with those reported for the 90+% AlF_3 samples of McVicker *et al.* (*17*). Apparently the fully fluorinated alumina, AlF_3, contains larger crystallites on average than the partially fluorinated alumina, $Al_2O_3(F)$.

The XRD pattern of the $Al_2O_3(DF)$ powder sample indicated the presence of mainly α-AlF_3. The difference in the XRD peak intensities between AlF_3 and $Al_2O_3(DF)$ samples may be ascribed to different preferred orientations of α-AlF_3 in the two samples. The average crystallite size was calculated to be 155 Å using the width of the intense (220) X-ray line. Thus fully fluorinated aluminas prepared by treatment with CHF_3 or HF have similar crystal structures (α-AlF_3 phase), extents of fluorination (90+%), crystallite sizes (155 Å), surface areas, and more importantly, similar surface chemistry (see below).

BET surface areas of various alumina samples are shown in Table 1. The average surface area of the γ-Al_2O_3 was calculated to be ca. 200 m^2/g. The average surface areas of fully fluorinated aluminas, AlF_3 and $Al_2O_3(DF)$, were one order of magnitude lower. The partially fluorinated material, $Al_2O_3(F)$, exhibited a surface area in between these two extremes, as expected.

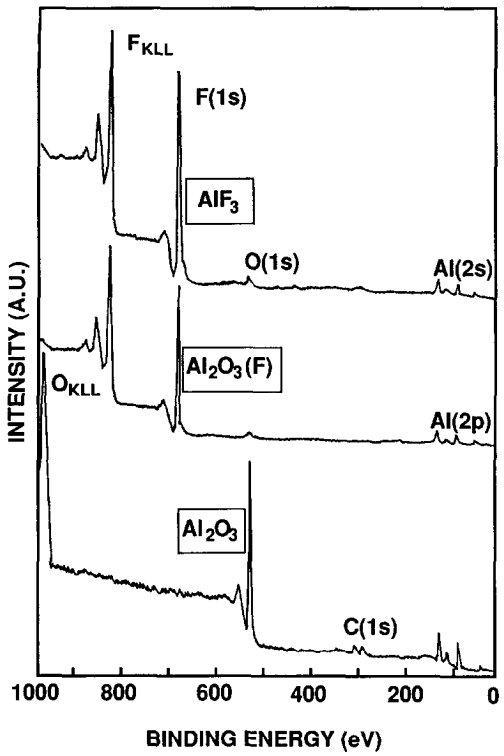

FIG. 2. XPS survey scans for (a) γ-Al_2O_3, (b) $Al_2O_3(F)$, and (c) AlF_3 samples.

The decrease in BET surface area is consistent in direction but not in magnitude with the increase in crystallite sizes determined by XRD. This suggests that other mechanisms of surface area loss, such as pore plugging by transport of volatile aluminum fluorides, may also operate during the fluorination process.

XPS spectra of the various alumina samples are shown in Fig. 2. Figure 2a, the representative spectrum of Al_2O_3, shows strong Al(2*p*), O(1*s*), and O(AES) signals for Al_2O_3. Figure 2b is the representative spectrum of $Al_2O_3(F)$, showing strong signals for the F(1*s*), F(AES), Al(2*p*), and Al(2*s*) peaks. Both the O(1*s*) and O(AES) signals were strongly attenuated on the $Al_2O_3(F)$ surface compared with that of the original oxide. Figure 2c, the representative spectrum for AlF_3, is quite similar to that of the $Al_2O_3(F)$ sample. Comparison of AlF_3 and $Al_2O_3(F)$ clearly suggests that the $Al_2O_3(F)$ surface is nearly completely fluorinated. Little carbon was observed on any of the fluorinated samples. Thus relatively high purity fluorinated aluminas can be prepared by using fluoroalkanes as fluorinating agents.

Detailed Al(2*p*) XPS spectra were recorded for pure alumina, partially fluorinated alumina, and fully fluorinated alumina samples. As shown in Fig. 3a, the Al(2*p*) spectrum of Al_2O_3 showed a single symmetric peak around 74.7 eV with a full-width-at-half-maximum of 2.9 eV. This is characteristic of Al_2O_3 (*23*). The Al(2*p*) spectrum of $Al_2O_3(F)$ showed a single symmetric peak around 76.8 eV with a fwhm of 2.9 eV (see Fig. 3b). Thus there was a shift of 2.1 eV for the Al(2*p*) peak compared to that of Al_2O_3, although the peak width did not change. This shift is characteristic of AlF_3 and in good agreement with literature values (*16, 22*). It appears that an Al(2*p*) signal typical of AlF_3 is observed for the partially fluorinated alumina. The conclusion that the partially fluorinated samples is completely fluorinated at the surface is further supported by the F/Al atomic ratio calculation. An F/Al atomic ratio of 2.8 was

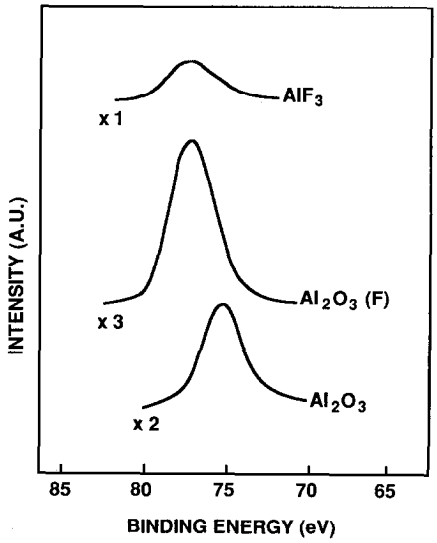

FIG. 3. Al(2*p*) spectra for (a) γ-Al_2O_3, (b) $Al_2O_3(F)$, and (c) AlF_3 samples.

obtained for the $Al_2O_3(F)$ sample [using Eq. (2) below]; this value is within the experimental error of the value expected for stoichiometric AlF_3. Thus from the Al(2*p*) peak location, peak symmetry, and the F/Al atomic ratio measurements, it may be concluded that: (1) The surface of $Al_2O_3(F)$ is mainly AlF_3; (2) fluorination essentially covers the alumina with a layer of AlF_3; and (3) the $Al_2O_3(F)$ surface does not appear to contain the segregated domains of Al_2O_3 and AlF_3 detected in the bulk by XRD. As shown in Fig. 3c, the Al(2*p*) spectrum of AlF_3 exhibited a single symmetric peak (fwhm of 2.9 eV) centered at 77.2 eV. This is in excellent agreement with the Al(2*p*) binding energy value of 77.3 for AlF_3 reported by Kerkhof *et al.* (*22*). XPS spectra of fluorinated aluminas prepared using non-CHF_3 sources, calcined at 873 K, were reported by Scokart *et al.* (*16*). The Al(2*p*) peaks for fluorinated aluminas (with fluorine contents higher than 20 wt%) were broad and asymmetric, indicating the presence of mixtures of Al_2O_3 and AlF_3. Kerkhof *et al.* studied the XPS of aluminas containing different amounts of fluorine introduced by the VKF process (which utilizes ammonium fluoride as the fluorinating agent) (*22*). In samples with fluorine contents higher than 20 at.%, Al(2*p*) line splitting and broadening were observed. They also concluded that this feature was due to the presence of two types of aluminum compounds in the samples (*22*).

O(1*s*) spectra of pure alumina (Fig. 4a), showed a broad peak (with fwhm of 3.5 eV) centered around 531.7 eV, characteristic of Al_2O_3 (*23*). The broadening of the O(1*s*) peak was likely due to the presence of surface OH groups on the alumina. The presence of surface OH groups on alumina has been well documented by several workers using IR techniques (*24–26*). As shown in Fig. 4b, the O(1*s*) spectrum of $Al_2O_3(F)$ exhibited two broad peaks centered around 533.6 and 527.6 eV. The appearance of two well-separated O(1*s*) peaks suggests the presence of at least two (possibly more)

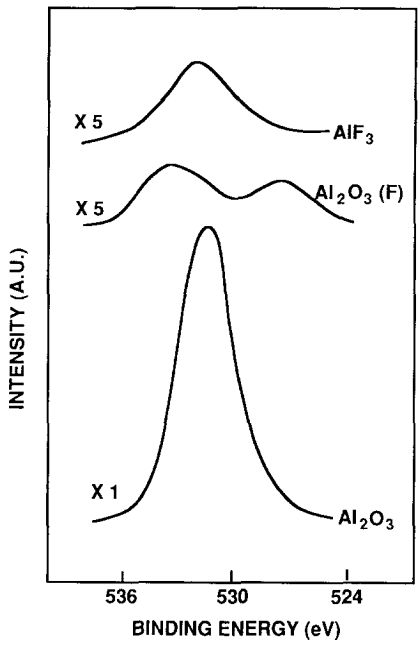

FIG. 4. O(1*s*) spectra for (a) γ-Al_2O_3, (b) $Al_2O_3(F)$, and (c) AlF_3 samples.

types of oxygen-containing surface species. These species can be attributed to O-containing ligands combined with Al and F. The possibilities include AlOF, AlFOH, AlF_2OH, and $[AlF_3OH]H$ species. That is, both Lewis acid (AlF_3 or Al–F species) and Brønsted acid (OH groups) functions may be present on partially fluorinated alumina. Both aprotic and protic species, if present, must have low volatility and high thermal stability, since pretreatment at 673 K in the UHV system produced no noticeable changes in the XPS spectrum. In contrast to the partially fluorinated alumina, O(1*s*) spectra of AlF_3 showed no distinct peaks, but merely a broad peak (with fwhm of 3.5 eV) centered about 532.8 eV. This may be due to the presence of water, since α-AlF_3 is hygroscopic in nature.

The atomic ratios for the various samples were computed from the area under the XPS peaks and use of the appropriate photoionization cross sections, accounting for the kinetic energy dependence (*27*) as shown in

$$\frac{n_A}{n_B} = \frac{I_A}{I_B} \times \frac{\sigma_A}{\sigma_B} (KE_B/KE_A)^{0.75}, \quad (1)$$

where I is the area under the XPS peak, σ is the photoionization cross section obtained from Scofield (*28*), and KE is the kinetic energy of the photoelectron.

The O(1*s*) spectra of Al_2O_3 and Al_2O_3(F), recorded under identical conditions, can be used to estimate the thickness of the AlF_3 overlayer (assumed to be uniform over the entire surface) from

$$I_x = I_O \exp[-X/\lambda \sin \theta], \quad (2)$$

where I_x is the O(1*s*) peak area in Al_2O_3(F), I_O is the O(1*s*) peak area in Al_2O_3, X is the thickness of the fluoride layer, and θ is the average escape angle of 50° for this instrument. Based on the equation by Seah and Dench (*29*),

$$\lambda = 2170E^{-2} + 0.72(aE)^{1/2}, \quad (3)$$

we calculate a mean free path (λ) of approximately 20 Å for the 954-eV O(1*s*) electron in Al_2O_3. With these assumptions the fluoride layer prepared by fluoroalkane treatment is estimated to be about 50 Å thick on the Al_2O_3(F) surface. Note that this represents a lower limit, since both O(1*s*) peaks were taken into account in the above Eq. (2).

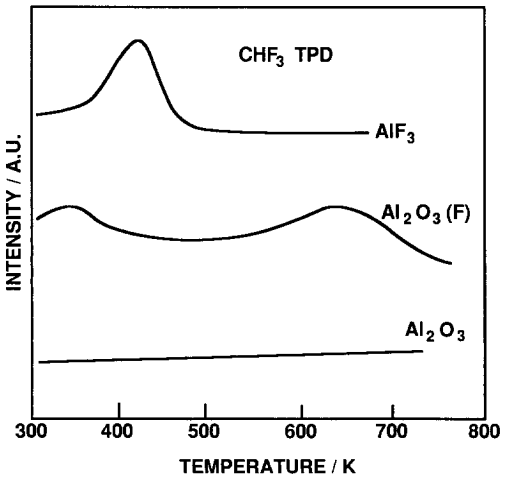

FIG. 5. TPD spectra for CHF_3 desorption from (a) γ-Al_2O_3, (b) Al_2O_3(F), and (c) AlF_3, following adsorption at 300 K.

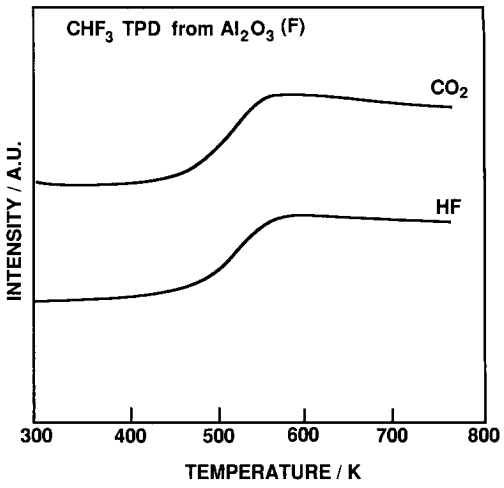

FIG. 6. Desorption of HF and CO_2 from CHF_3 TPD on Al_2O_3(F).

Reactions of CHF_3 on Fluorinated Aluminas

No detectable CHF_3 adsorption occurred on the γ-alumina powder at room temperature. Exposure of the alumina to CHF_3 at 300 K and subsequent TPD produced no desorption of CHF_3 or of any reaction products, as shown in Fig. 5a.

In contrast, CHF_3 adsorption on the Al_2O_3(F) powder at 300 K and subsequent TPD gave CHF_3, HF, and CO_2 desorption signals. HF and CO_2 (see Fig. 6) were the major decomposition products from CHF_3 on Al_2O_3(F). CHF_3 desorbed in an intense peak around 625 K (Fig. 5b). CHF_3 desorption from the Al_2O_3(F) most likely involved more than one adsorbed state. There was also a less intense, low-temperature CHF_3 peak evident as a shoulder in the 300–400 K temperature range. A similar low-temperature peak was observed following adsorption on the highly fluorinated samples (see below). HF and CO_2 desorbed around 550 K. Carbon deposits were apparent from the gray color of the Al_2O_3(F) powder after the temperature ramp was stopped at 800 K and the sample was cooled to room temper-

ature. No other desorption and/or decomposition products were observed in the temperature range 300 to 800 K. Other possible products searched for, but not found, were CF_4, H_2, C_2F_4, C_2F_6, F_2, and C_2HF_5. From a first-order Redhead analysis (*30*) using a preexponential factor of 10^{13} sec^{-1}, the estimated activation energy for desorption (E_d) of CHF_3 from the state at 625 K is 43.5 kcal/mol. TPD confirmed that CHF_3 reacts on $Al_2O_3(F)$ as evidenced by HF and CO_2 desorption at lower temperatures than CHF_3 desorption. In the TPD experiments, HF onset began as low as 450 K; this implies that CHF_3 dissociates either during adsorption at 300 K or during the temperature ramp below 450 K.

CHF_3 adsorption on the AlF_3 powder surface at 300 K and subsequent TPD produced only CHF_3 desorption in a single peak around 420 K (Fig. 5c). No other molecular species such as dissociation and/or desorption products of CHF_3 were seen on AlF_3. Potential products such as H_2, HF, C_2F_4, C_2HF_5, and C_2F_6 were carefully checked for, but not found in the TPD runs over the temperature range 300–800 K. The activation energy for molecular CHF_3 desorption was calculated to be 28.9 kcal/mol using the experimental value of T_p = 420 K and assuming first-order desorption kinetics with $\nu = 10^{13}$ sec^{-1}.

CHF_3 adsorption on the Al_2O_3(DF) powder surface at 300 K and subsequent TPD also yielded only CHF_3 desorption around 400 K (not shown). The desorption peak was approximately 20 K lower on the Al_2O_3(DF) surface than that on the AlF_3 surface, and was less well resolved. No other desorption and/or decomposition products of CHF_3 were found. As on AlF_3, CHF_3 exposure to the Al_2O_3(DF) surface at room temperature resulted in only molecular adsorption, with no reaction or decomposition.

The desorption temperature of CHF_3 from $Al_2O_3(F)$ was considerably higher (625 K) than that from AlF_3 (420 K), indicating stronger binding of CHF_3 on $Al_2O_3(F)$. At 300 K, CHF_3 adsorption on partially fluorinated alumina most likely involves both molecular and dissociated states, while on fully fluorinated alumina adsorption appears to be molecular. Thus there is a marked difference between the adsorption–desorption behavior of CHF_3 on $Al_2O_3(F)$ and that of AlF_3, the latter inhibiting dissociation and producing a shift of the desorption peak to much lower temperatures. The activation energy for desorption of CHF_3 was significantly higher (ca. 15 kcal/mol) for the partially fluorinated alumina.

The connection between the sample pretreatment time, i.e., the fluorine content of the sample, and the capacity for CHF_3 chemisorption was therefore investigated in greater detail. The high-temperature CHF_3 desorption peak area can be used as a measure of surface reactivity. The relative changes in the high-temperature CHF_3 peak area as a function of the fluorination time at 773 K of a series of alumina samples are illustrated in Fig. 7. In these experiments, a series of aluminas was fluorinated to different extents (0 to 90+%), followed by a saturation CHF_3 exposure at 300 K for each subsequent TPD run. As shown in Fig. 7, the total intensity of the CHF_3 peak at ca. 600 K initially increases rapidly with sample fluorination and then passes

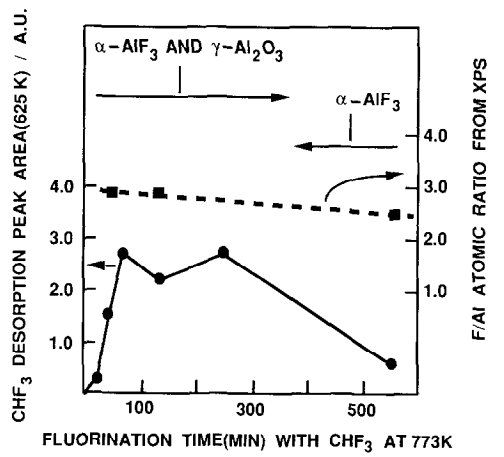

FIG. 7. Variation with fluorination time of the activity of partially fluorinated alumina for strong CHF_3 adsorption.

through a broad maximum (between 50–250 min); finally the desorption signal decreases slowly with further increase in fluorination time. The maximum CHF_3 desorption signal was observed at intermediate fluorination times. At these intermediate fluorination times the samples consisted of both unreacted γ-alumina and detectable amounts of α-AlF_3, as evidenced by XRD. At fluorination times greater than ca. 400 min the sample was α-aluminum fluoride with an approximately 90% reduction in surface area (compared to that of pure alumina). Fully fluorinated alumina showed a clear activity loss for strong adsorption of CHF_3. However, XPS results indicated a high degree of fluorination of the alumina surface even at very short fluorination times.

Halogen Exchange With Chlorofluorocarbons on Partially Fluorinated Alumina

All of the above results suggest that only partially fluorinated alumina samples are active for strong adsorption of CHF_3 at room temperature. Further investigations of the interactions of other CFCs (HCFC-22, HCFC-21, and CFC-12) with Al_2O_3(F) at room temperature was therefore conducted using mainly TPD. The reaction products may be grouped as gaseous products and solid products. The gaseous products were analyzed by mass spectrometry in accordance with their mass spectral cracking patterns (*31, 32*). The solid products were analyzed using XPS and XRD. The principal findings are described below.

$CHClF_2$ adsorption on the Al_2O_3(F) powder surface at 300 K and subsequent TPD resulted in $CHClF_2$, CHF_3, HF, and CO_2 desorption. Twenty-two different masses corresponding to likely desorption products were examined in the TPD experiments: 2(H_2), 18(H_2O), 20(HF), 36(HCl), 38(F_2), 44(CO_2), 51($CHClF_2$, CHF_3, C_2HF_3), 54(ClF), 63(C_2HF_3), 64($C_2H_2F_2$), 67 ($CHCl_2F$), 69(CHF_3, CF_4, $CHCl_2F$, C_2F_6, $CClF_3$), 70(Cl_2), 81(C_2F_4), 82(C_2HF_3), 83($CHCl_3$), 85($CClF_3$, CCl_2F_2, $C_2H_2F_4$), 92(ClF_3), 101(CCl_3F), 102($C_2H_2F_4$), 117 (CCl_4), and 119(C_2F_6). The desorption peaks for masses 2, 36, 38, 54, 63, 64, 70, 81, 82, 83, 85, 92, 101, 102, 117, and 119 were carefully checked, but not found in TPD runs over the temperature range 300–800 K. The only desorption signals found in TPD were the peaks for m/e = 20, 44, 51, and 69. The desorption peak for mass 69 was assigned to CHF_3, while the peak for mass 51 was primarily $CHClF_2$ desorption. Mass 20 was due to HF and 44 to CO_2 desorption.

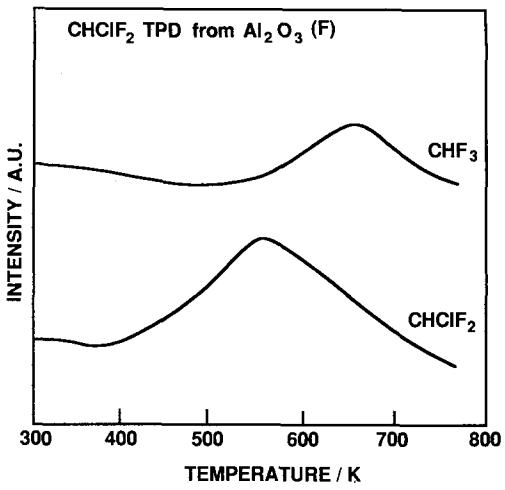

FIG. 8. Desorption of $CHClF_2$ and CHF_3 following $CHClF_2$ adsorption on Al_2O_3(F) at 300 K.

As shown in Fig. 8, $CHClF_2$ desorbed in a broad peak around 550 K. CHF_3 resulting from the reaction of $CHClF_2$ desorbed as a single peak at higher temperature (around 650 K). HF and CO_2, which were also decomposition products (not shown in the figure), desorbed around 550 K. Residual carbon deposits were apparent on the Al_2O_3(F) surface after the temperature ramp was stopped at 800 K and the sample was cooled to room temperature. By assuming first-order reaction kinetics the activation energy for the chemisorbed $CHClF_2$ desorption may be estimated to be 38.2 kcal/mol; that for CHF_3 is comparable to the value obtained after CHF_3 adsorption,

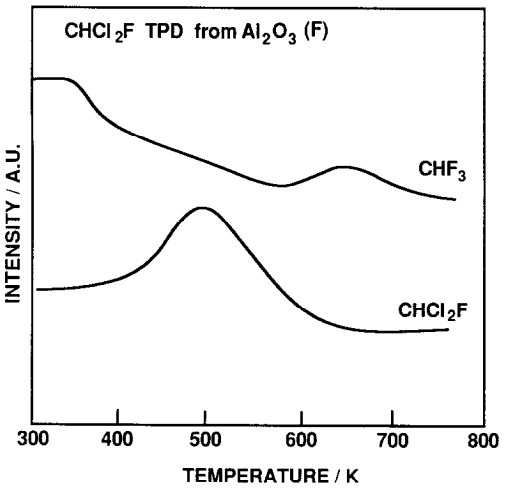

FIG. 9. Desorption of $CHCl_2F$ and CHF_3 following $CHCl_2F$ adsorption on $Al_2O_3(F)$ at 300 K.

indicating that evolution of this product was limited by its desorption kinetics.

$CHClF_2$ adsorbed relatively strongly on the $Al_2O_3(F)$ surface at room temperature as evidenced by the $CHClF_2$ desorption at 550 K. A significant fraction of the $CHClF_2$ adsorbed on the $Al_2O_3(F)$ surface reacted, as evidenced by the desorption of HF, CO_2, CHF_3, and the presence of residual carbon. Desorption of CHF_3 from $Al_2O_3(F)$ clearly indicates that (1) further fluorination of $CHClF_2$ to CHF_3 occurred on the $Al_2O_3(F)$ surface; (2) $CHClF_2$ did not undergo disproportionation into CHF_3 and $CHCl_3$; (3) $CHClF_2$ did not undergo C–C bond-forming reactions, e.g., to C_2F_4 and HCl.

$CHCl_2F$ also reacted on the $Al_2O_3(F)$ powder surface: adsorption at 300 K and subsequent TPD resulted in $CHCl_2F$, CHF_3, and HF desorption. As shown in Fig. 9, $CHCl_2F$ desorbed as a single peak around 500 K. CHF_3 and HF were the major desorption/decomposition products of $CHCl_2F$ from the $Al_2O_3(F)$ surface. CHF_3, the fluorinated product of $CHCl_2F$, desorbed as a single peak around 625 K. As in the $CHClF_2/Al_2O_3(F)$ experiments, 22 different masses were checked, but not found, in the TPD runs over the temperature range of this study. The detectable desorption signals found in the TPD study were peaks for m/e = 20, 44, 67, and 69. By comparison of mass spectra of CHF_3, $CHClF_2$, and $CHCl_2F$, the desorption signal for mass 67 was assigned to $CHCl_2F$, and 69 to CHF_3. CHF_3 can be produced from either $CHClF_2$ or $CHCl_2F$, but no $CHClF_2$ was detected from $CHCl_2F$. We were unable to detect production of HCl, $CHCl_3$, or $CHClF_2$ from $CHCl_2F$ mass spectrometrically.

The adsorbed $CHCl_2F$ decomposed on $Al_2O_3(F)$ as evidenced by the TPD results. To confirm this observation, XPS data were obtained from the $Al_2O_3(F)$ sample after several adsorption and desorption cycles. XPS detected Cl and C on the $Al_2O_3(F)$ surface in addition to the Al, O, and F originally present.

In contrast, no detectable CCl_2F_2 adsorption occurred on the $Al_2O_3(F)$ surface at 300 K. TPD following CCl_2F_2 exposure showed no CCl_2F_2 desorption and no evidence for any of the potential reaction products searched for above.

DISCUSSION

The fluorination procedure used here was quite similar to that described by McVicker *et al.* (*17*). These workers observed that (1) complete fluorination of alumina could be achieved with CHF_3 at 800 K; (2) the aluminum fluoride thus obtained was the α-AlF_3 phase with approximately 150-Å crystallite sizes; and (3) the surface area of the fluorinated alumina decreased with increasing fluorination. Similar characteristics were observed in the present experiments.

The reactivity of fluorinated aluminas was evaluated based on CHF_3 chemisorption and the powder TPD results. No CHF_3 adsorption occurred on pure alumina at room temperature. On AlF_3 as well as on $Al_2O_3(F)$, CHF_3 adsorbed at room temperature, but the adsorption was weak and molecular. CHF_3 adsorbed strongly and dissociatively on the $Al_2O_3(F)$ surface at room temperature as evidenced by a major

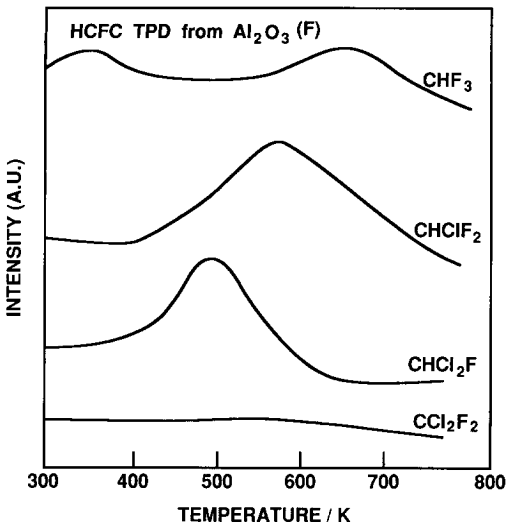

FIG. 10. Comparison of desorption spectra of C_1-HCFCs for adsorption of each on Al_2O_3(F) at 300 K.

CHF_3 desorption peak at higher temperature (625 K) and desorption of decomposition products of CHF_3 (HF and CO_2) at lower temperatures. Thus there is a marked difference in the surface chemistry of CHF_3 on partially fluorinated alumina and fully fluorinated alumina. Complete fluorination of alumina inhibits the dissociative adsorption of CHF_3 and shifts the CHF_3 desorption maximum from 625 to 420 K. The activation energy for desorption is decreased by ca. 15 kcal/mol. Thus there is clear evidence for formation of active sites on partially fluorinated alumina. This material also shows activity for chlorine-for-fluorine exchange reactions of the other HCFCs examined, with no evidence for replacement of the hydrogen in these molecules. While the nature of the active sites for these reactions is not evident from this work, the partially fluorinated materials which are active are analogous to those on which other workers (*12, 15–17, 33*) have observed strong Brønsted activity.

It is interesting to compare the adsorption of CHF_3, $CHClF_2$, $CHCl_2F$, and CCl_2F_2 on the partially fluorinated alumina at room temperature. The adsorption behavior, desorption kinetics, and identity of desorption products derived from the TPD results provide insight into the chemical processes taking place on this alumina surface. These also suggest that TPD may be effective as a method for screening a large number of potential intermediates and routes for HCFC production. They also suggest a possible role of fluorinated aluminas as HCFC reservoirs for recycling applications, since HCFCs appear to be strongly bound. In contrast to the fully halogenated CFC-12, all the HCFCs adsorbed strongly and dissociatively at room temperature on partially fluorinated alumina, as evidenced by the desorption of the parent molecule at higher temperature and by the desorption of the reaction products such as CHF_3 and HF. Carbon and chlorine deposits were detected in the XPS examination of the Al_2O_3(F) surface after the desorption runs. TPD showed characteristic but different desorption temperatures for CHF_3, $CHClF_2$, and $CHCl_2F$. As shown in Fig. 10 and Table 3, the desorption temperature decreased in the order $CHF_3 > CHClF_2 > CHCl_2F$. The activation energy for desorption decreased by ca. 5 kcal/mol for each F replaced by Cl in these HCFCs. This is a surprisingly large difference to be accounted for by a purely inductive effect and may reflect direct fluorine-bonding to the surface, as suggested by Taylor and Cheung (*34*). However, some interaction with the surface via the hydrogen in these HCFCs, whether dissociative or not, must also occur, as CCl_2F_2 does not adsorb at 300 K on any of the materials examined in this study.

TABLE 3

Desorption of HCFCs from Partially Fluorinated Alumina, Al_2O_3(F)

Product	T_p (K)	E_d (kcal/mol)
CHF_3	625	43.5
$CHClF_2$	550	38.2
$CHCl_2F$	500	34.6
CCl_2F_2	<300	

The desorption of CHF_3 at the same temperature, regardless of its origin, indicates that the evolution of this product from $CHClF_2$ and $CHCl_2F$ is limited by the kinetics of desorption. This phenomenon may also account for the halogen exchange selectivity observed for the reaction of $CHCl_2F$: there was no evidence for $CHClF_2$ formation which might be expected enroute to CHF_3. The preferential formation of CHF_3 may be driven by its stronger interaction with the fluorinated alumina surface. To the extent that this conclusion may be generalized to other halogen exchange reactions, adsorption thermodynamics are likely to play a critical role in the selective synthesis of CFC alternatives.

CONCLUSIONS

Chlorine-for-fluorine exchange of the C_1-HCFCs $CHClF_2$ and $CHCl_2F$ was observed in TPD experiments with partially fluorinated aluminas. CHF_3 was the only fluorocarbon product of these reactions, and was evolved with desorption-limited kinetics. Only partially fluorinated aluminas were active for reaction of the C_1-HCFCs; γ-Al_2O_3 and α-AlF_3 individually exhibited no activity for decomposition of CHF_3 adsorbed at 300 K. In contrast, none of these materials exhibited activity for adsorption or reaction of fully halogenated species such as CCl_2F_2 at 300 K. These results suggest that selective fluorine-for-chlorine exchange in HCFCs can be accomplished with partially fluorinated aluminas, although the details of this reaction are far from resolved.

ACKNOWLEDGMENTS

We gratefully acknowledge the support of this research by the National Science Foundation (Grant CBT-8451055) and by E. I. du Pont de Nemours & Co., Inc. We would like to thank L. E. Manzer and D. R. Corbin for introducing us to this subject, and for providing the alumina sample used in this work. D. S. Lafyatis performed the surface area measurements.

REFERENCES

1. *Science* **239,** 1489 (1988).
2. *Chem. Eng. News,* April 4, 1988.
3. *Science* **242,** 666 (1988).
4. Manzer, L. E., and Rao, V. N. M., U.S. Pat. 4,766,260 (1988).
5. Miller, C. B., and Calfee, J. D., U.S. Pat. 2,748,177 (1957).
6. Stacey, M., Tatlow, J. C., and Sharpe, A. G., "Advances in Fluorine Chemistry," Vol. 3. Butterworths Washington, DC, 1963.
7. Holm, V. C. F., and Clark, A., *Ind. Eng. Chem. Prod. Res. Dev.* **2,** 38 (1963).
8. Covini, R., Fattore, V., and Giordano, N., *J. Catal.* **7,** 126 (1967).
9. Gerberich, H. R., Lutinski, F. E., and Hall, W. K., *J. Catal.* **6,** 209 (1966).
10. Bulgakov, O. V., and Antipina, T. V., *Kinet. Katal.* **9,** 1059 (1968).
11. Antipina, T. V., Bulgakov, O. V., and Uvarov, A. V., *in* "Proceedings, 4th International Congress on Catalysis, Moscow, 1968" (B. A. Kazansky, Ed.), Vol. 2, p. 306. Akademiai Kiado, Budapest, 1971.
12. Reitsma, H. J., and Boelhouwer, C., *J. Catal.* **33,** 39 (1974).
13. Covini, R., Fattore, V., and Giordano, N., *J. Catal.* **9,** 315 (1967).
14. Holm, V. C. F., and Clark, A., *J. Catal.* **8,** 286 (1967).
15. Kerkhof, F. P. J. M., Oudejeans, J. C., Moulijn, J. A., and Matulewicz, E. R. A., *J. Colloid Interface Sci.* **77,** 120 (1980).
16. Scokart, P. O., Selim, A., Damon, J. P., and Rouxhet, P. G., *J. Colloid Interface Sci.* **70,** 209 (1979).
17. McVicker, G. B., Kim, C. J., and Eggert, J. J., *J. Catal.* **80,** 315 (1983).
18. Amphlett, J. L., Coomber, J. W., and Whittle, E., *J. Phys. Chem.* **70,** 593 (1966).
19. Kim, K. S., Barteau, M. A., and Farneth, W. E., *Langmuir* **4,** 533 (1988).
20. Klug, H. P., and Alexander, L. E., "X-ray Diffraction Procedures for Polycrystalline and Amorphous Materials," 2nd ed. Wiley, New York, 1974.
21. Moerkerken, A., Behr, B., Noordeloos-Maas, M. A., and Boelhouwer, C., *J. Catal.* **24,** 177 (1972).
22. Kerkhof, F. P. J. M., Reitsma, H. J., and Moulijn, J. A., *React. Kinet. Catal. Lett.* **7,** 15 (1977).
23. Perkin–Elmer Co., Physical Electronics Div., "Handbook of X-ray Photoelectron Spectroscopy." Minnesota, 1979.
24. Peri, J. B., *J. Phys. Chem.* **69,** 220 (1965).
25. Knözinger, H., and Ratnasamy, P., *Catal. Rev. Sci. Eng.* **17,** 31 (1978).
26. Okamoto, Y., and Imanaka, T., *J. Phys. Chem.* **92,** 7102 (1988).
27. Powell, C. J., *Surf. Sci.* **44,** 29 (1974).
28. Scofield, J. H., *J. Electron. Spectrosc. Relat. Phenom.* **8,** 129 (1976).

29. Seah, M. P., and Dench, W. A., *Surf. Interface. Anal.* **1,** 2 (1972).
30. Redhead, P. A., *Vacuum* **12,** 203 (1962).
31. Cornu, A., and Massot, R., "Compilation of Mass Spectral Data." Heyden, London, 1966.
32. Mass Spectrometry Data Centre, "Eight Peak Index of Mass Spectra," 2nd ed. Aldermaston, Reading, England, 1974.
33. Murrell, L. L., and Dispenziere, N. C., *J. Catal.* **117,** 275 (1989).
34. Taylor, M. D., and Cheung, T.-T., *J. Inorg. Nucl. Chem.* **35,** 3499 (1973).